

High Turnover of Tissue Factor Enables Efficient Intracellular Delivery of Antibody–Drug Conjugates

Bart E.C.G. de Goeij¹, David Satijn¹, Claudia M. Freitag¹, Richard Wubbolts², Wim K. Bleeker¹, Alisher Khasanov³, Tong Zhu³, Gary Chen³, David Miao³, Patrick H.C. van Berkel¹, and Paul W.H.I. Parren^{1,4,5}

Abstract

Antibody–drug conjugates (ADC) are emerging as powerful cancer treatments that combine antibody-mediated tumor targeting with the potent cytotoxic activity of toxins. We recently reported the development of a novel ADC that delivers the cytotoxic payload monomethyl auristatin E (MMAE) to tumor cells expressing tissue factor (TF). By carefully selecting a TF-specific antibody that interferes with TF:FVIIa-dependent intracellular signaling, but not with the procoagulant activity of TF, an ADC was developed (TF-011-MMAE/HuMax-TF-ADC) that efficiently kills tumor cells, with an acceptable toxicology profile. To gain more insight in the efficacy of TF-directed ADC treatment, we compared the internalization characteristics and intracellular routing of TF with the EGFR and HER2. Both in absence and presence of antibody, TF demonstrated more efficient internalization, lysosomal targeting, and degradation than EGFR and HER2. By conjugating TF, EGFR, and HER2-specific antibodies with duostatin-3, a toxin that induces potent cytotoxicity upon antibody-mediated internalization but lacks the ability to induce bystander killing, we were able to compare cytotoxicity of ADCs with different tumor specificities. TF-ADC demonstrated effective killing against tumor cell lines with variable levels of target expression. In xenograft models, TF-ADC was relatively potent in reducing tumor growth compared with EGFR- and HER2-ADCs. We hypothesize that the constant turnover of TF on tumor cells makes this protein specifically suitable for an ADC approach. *Mol Cancer Ther*; 14(5); 1130–40. ©2015 AACR.

Introduction

Therapeutic antibodies are currently used in the clinic to treat a variety of diseases, including cancer. The tumor-killing capacity of therapeutic antibodies can be greatly enhanced by conjugation with cytostatic toxins, this way combining antibody-mediated tumor targeting with the potent cytotoxic activity of toxins. This was also demonstrated through the FDA approval of brentuximab vedotin, a CD30-specific antibody coupled to the potent microtubule disrupting agent monomethyl auristatin E (MMAE), for the treatment of patients with Hodgkin lymphoma or anaplastic T-cell lymphoma (1). In addition, the approval of trastuzumab emtansine (T-DM1), an antibody–drug conjugate (ADC) composed of the HER2 antibody trastuzumab and the tubulin

inhibitor maytansine (DM1), for the treatment of patients with HER2-positive breast cancer (2, 3) emphasizes that the potential of ADCs is not limited to hematological malignancies. The number of ADCs in clinical development has markedly increased in the last couple of years. This includes the development of HuMax-TF-ADC (TF-011-MMAE), a novel ADC designed to deliver the cytotoxic payload MMAE to tumor cells expressing tissue factor (TF; ref. 4).

TF, also called thromboplastin, factor III, or CD142, is aberrantly expressed in many types of cancers, including non-small cell lung cancer (5), colorectal cancer (6), genito-urethral (7, 8), and gynecologic cancers (9–11), pancreatic cancer (12), head and neck cancer (13), glioma (14), and metastatic breast cancer (15). Under physiologic conditions, TF is expressed by fibroblasts, pericytes, and smooth muscle cells in the subendothelial vessel wall. In these cells, the majority of TF is localized in intracellular pools and remains sequestered from circulating factor VII (FVII) until vascular integrity is disrupted or until TF expression is induced (16–18). Upon vascular damage, TF binds activated FVII (FVIIa) and forms the proteolytically active TF:FVIIa complex that can initiate the coagulation pathway. The TF:FVIIa complex can also activate cells by cleavage of the G-protein coupled receptor protease-activated receptor 2 thereby inducing an intracellular signaling cascade that promotes proliferation, thrombosis, and angiogenesis (19). This makes TF an interesting yet challenging target for cancer immunotherapy.

TF-011-MMAE was designed to specifically target tumor cells that aberrantly express TF, without interfering with the role of TF in coagulation. TF-011-MMAE showed potent antitumor

¹Genmab, Utrecht, the Netherlands. ²Department of Biochemistry and Cell Biology, Faculty of Veterinary Medicine, Utrecht University, Utrecht, the Netherlands. ³Concortis Biosystems Corp., San Diego, California. ⁴Department of Cancer and Inflammation Research, Institute of Molecular Medicine, University of Southern Denmark, Odense, Denmark. ⁵Department of Immunohematology and Blood Transfusion, Leiden University Medical Center, Leiden, the Netherlands.

Note: Supplementary data for this article are available at Molecular Cancer Therapeutics Online (<http://mct.aacrjournals.org/>).

Corresponding Author: Bart E.C.G. de Goeij, Genmab B.V., Yalelaan 60, 3584CM Utrecht, the Netherlands. Phone: 31-302123181; Fax: 31-302123110; E-mail: BGO@genmab.com

doi: 10.1158/1535-7163.MCT-14-0798

©2015 American Association for Cancer Research.

activity in xenograft models derived from a broad range of solid cancers, and an acceptable safety profile in nonclinical toxicity studies (4). TF-011-MMAE and unconjugated TF-011 induced efficient antibody-dependent cell-mediated cytotoxicity and inhibition of TF:FVIIa-dependent intracellular signaling, both of which may contribute to the antitumor activity of TF-011-MMAE. However, MMAE-mediated tumor cell killing was shown to be the dominant mechanism of action *in vivo*. This indicates that TF is a highly suitable target for the intracellular delivery of cytotoxic agents through an ADC. To gain more insight in the target characteristics, particularly the internalization characteristics of TF and TF-specific antibodies, that contribute to the efficacy of TF-directed ADC treatment, we compared TF-specific ADCs with ADCs directed against HER2 and EGFR. HER2 is a well-known and clinically validated ADC target (3, 20), and an EGFR antibody conjugated with DM1 through a noncleavable linker system is currently being evaluated in a phase I clinical study. Antibodies targeting TF, HER2, and EGFR were conjugated with the cytotoxic compound duostatin-3, which blocks tubulin polymerization. This toxin lacks the ability to induce bystander killing and therefore only affects target-positive cells. Because tumor antigens are often heterogeneously expressed and therefore not always accessible to ADC treatment, an ADC capable of inducing bystander killing may be preferred from an efficacy point-of-view (4). However, to study the target requirements needed for optimal intracellular delivery of cytotoxic agents, we selected a drug-linker combination that only affects antigen expressing cells.

By comparing *in vitro* and *in vivo* cytotoxicity of ADCs targeting TF, HER2, and EGFR, we found that TF-ADC was more effective compared with ADCs targeting the EGF-receptor family. TF-ADC induced relatively potent tumor cell killing, even in cell lines where TF expression was lower than expression of HER2 or EGFR. Confocal microscopy analysis demonstrated faster and enhanced transport of TF-antibodies into lysosomes of tumor cells compared with EGFR and HER2 antibodies. Strikingly, also without antibody treatment, large quantities of TF were found to internalize and colocalize with markers of endosomes and lysosomes, indicating that TF was constitutively being replenished. Therefore, it seems that the high turnover of TF on tumor cells, inherent to its biologic role, makes this protein specifically suitable for an ADC approach.

Materials and Methods

Cell lines

Human SK-OV-3 (ovarian cancer), AU565 (breast adenocarcinoma), and HCC1954 (breast ductal carcinoma) cells were obtained from ATCC. Human A431 (epithelial squamous carcinoma) and Jurkat (T-cell leukemia) cells were obtained from the Deutsche Sammlung von Mikroorganismen und Zellkulturen (DSMZ). SK-OV-3 cells were cultured in Minimal Essential Medium Eagles (ATCC) containing 10% heat-inactivated calf serum (Hyclone). HCC1954, A431, and Jurkat cells were cultured in RPMI-1640 (Lonza) containing 10% heat-inactivated calf serum. AU565 cells were cultured in RPMI-1640 supplemented with 10% heat-inactivated calf serum, 1% sodium bicarbonate (Lonza), 0.5% natrium pyruvate (Lonza), and 0.5% glucose (Sigma). To guarantee cell line authenticity, cell lines were aliquoted and banked, and cultures were grown and used for a limited number of passages before starting a new culture from stock. Cell lines were routinely tested for mycoplasma contamination. TF, HER2, and EGFR cell surface expres-

sion was quantified by QIFIKIT analysis (DAKO) according to the manufacturer's guidelines, using a mouse anti-human TF antibody (CLB), mouse anti-human HER2 antibody (R&D), and mouse anti-human EGFR antibody (BD) as described in Supplementary Method S1.

Antibody generation and conjugation

Human IgG1 κ monoclonal antibodies were generated in human antibody transgenic mice; HuMAb mice (Medarex), using hybridoma technology (21). TF antibodies were previously described (4). In brief, TF-011 binds TF, interferes with FVIIa binding, and inhibits ERK phosphorylation. TF-111 binds TF and partially interferes with FVIIa binding and ERK-phosphorylation. The HER2 mAbs 153 and 005 were described by (22). Both antibodies bound to epitopes distinct from those recognized by trastuzumab and pertuzumab. Upon binding to HER2, mAb 153 inhibits ligand-induced HER2 proliferation. mAb 005 has no effect on HER2-induced proliferation. The EGFR mAbs zalutumumab and nimotuzumab (Biacon) both inhibit ligand-binding and EGFR-driven proliferation. Zalutumumab does so with high affinity (23), whereas nimotuzumab blocks EGF binding with low affinity (24).

Duostatin-3-conjugated antibodies were generated by covalent conjugation of valine-citrulline-duostatin-3 on antibody lysine groups as described in WO/2013/173391. The synthesis of duostatin-3 is also described in the Supplementary Method S2. Each resulting duostatin-3-conjugated ADC contained an average of two drug molecules per antibody, as determined by hydrophobic interaction chromatography. Duostatin-3-conjugated antibodies were referred to as TF-ADC, HER2-ADC, and EGFR-ADC. TF-011 was also conjugated with maleimido-caproyl-valine-citrulline-*p*-aminobenzoyl-monomethyl auristatin E (vcMMAE, licensed from Seattle Genetics) on cysteine groups in the antibody hinge region, to generate TF-011-MMAE (HuMax-TF-ADC), as described (4). This ADC was referred to as TF-011-MMAE throughout the article. TF-011-MMAE contained an average of four drug molecules per antibody.

Confocal microscopy

Cells were grown on glass coverslips (Thermo Fisher Scientific) at 37°C for 16 hours. In case of antibody stimulation, cells were preincubated 1 hour with 50 mg/mL leupeptin (Sigma) to block lysosomal activity followed by 1 or 16 hours incubation with 1 mg/mL EGFR-, HER2-, or TF-antibody. Cells were fixed, permeabilized, and incubated 45 minutes with mouse anti-human TF (CLB), HER2 (R&D), and EGFR (BD Pharmingen) antibodies, followed by goat anti-mouse IgG1-FITC (DAKO) to identify receptors, or goat anti-human IgG1-FITC (Jackson) to stain for human EGFR-, HER2-, and TF-antibodies. Endosomes were stained with rabbit anti-human transferrin (Life Technology) and goat anti-rabbit IgG-Alexa-568 (Bio-connect), lysosomes were stained with mouse anti-human CD107a-APC (BD). Finally, coverslips were mounted (Calbiochem) on microscope slides and imaged with a Leica SPE-II confocal microscope (Leica Microsystems) equipped with LAS-AF software. 12-bit grayscale TIFF images were analyzed for colocalization using MetaMorph software (Molecular Devices). Colocalization was calculated as the FITC pixel intensity overlapping with APC (lysosomes) or Alexa-Fluor568 (endosomes) and expressed as percentage of total FITC intensity.

Surface protein downmodulation assay

SK-OV-3 and A431 cells were seeded in 96-wells nonbinding plates (Greiner), 100,000 cells/well, in serum-free culture medium, with or without 100 mmol/L monensin (Dako) to block recycling of endosomes (30 minutes, 37°C; ref. 25). Next, human TF-, HER2-, and EGFR-antibodies (10 mg/mL), EGF (Biosource, 50 ng/mL) or FVIIa (Novoseven, 100 ng/mL) were added for 3 hours (37°C). Remaining TF, HER2, or EGFR at the plasma membrane was stained with noncompeting mouse TF (CLB), HER2 (R&D), and EGFR antibodies (BD; 30 minutes, 4°C), followed by incubation with goat anti-mouse IgG-FITC (Jackson, 30 minutes, 4°C). MFI of FITC was measured on a flow cytometer (BD). Quantification of cell surface proteins was done using QFIKIT (Dako) according to the manufacturer's instructions (26).

Total protein downmodulation assay

Cells were seeded (100,000 cells/well) in 96-wells culture plates (Greiner). After 4 hours, cells were preincubated with 100 mmol/L chloroquine (Sigma) or 100 mg/mL leupeptin (Sigma, 30 minutes, 37°C), followed by incubation with 10 mg/mL human TF, HER2, or EGFR antibodies. After 48 hours, cells were washed, lysed, and total protein levels were quantified using bicinchoninic acid protein assay reagent (Pierce), according to the manufacturer's instruction. Next, ELISA plates (Greiner) were coated with 1 mg/mL mouse anti-human EGFR (Millipore), rabbit anti-human HER2 (Cell Signaling Technology), or mouse anti-human TF (CLB), blocked with 2% chicken serum (Hyclone) and incubated with 50 mL cell lysate. Subsequently, EGFR, HER2, and TF were detected with mouse anti-human EGFR-biotin (Leica Technologies, 0.5 mg/mL), goat anti-human HER2-biotin (R&D, 50 ng/mL), and goat anti-human TF-biotin (R&D, 0.5 mg/mL). The reaction was visualized as described (27).

Intracellular antibody accumulation

Cells were incubated with 5 mg/mL FITC-conjugated antibodies at either 4°C or 37°C. At the indicated time points, cells were transferred on ice to stop internalization and washed with ice-cold PBS (B. Braun). Of note, 50 mL ice-cold acid wash buffer [0.2 mol/L glycine (Sigma), 4 mol/L urea (Sigma), pH2.0] was added for 5 minutes to remove extracellular bound antibodies and removed through centrifugation. Remaining FITC fluorescence, originating from internalized FITC-conjugated antibodies, was measured using flow cytometry.

CypHer5E internalization assay

Cells were seeded in 96-well plates (Greiner, 20,000 cells/well) and cultured overnight at 37°C. Ice-cold culture medium with or without 100 mmol/L chloroquine (Sigma) was added for 1 hour at 4°C, to trap internalized antibody in endosomal compartments. Next, 1 mg/mL HER2, EGFR, or TF antibody, conjugated with CypHer5E according to the manufacturer's instructions (GE Healthcare), was added. CypHer5E is a pH-sensitive dye which is nonfluorescent at basic pH (extracellular: culture medium) and fluorescent at acidic pH (intracellular: endosomes, lysosomes). After 30 minutes, the cells were washed and fresh culture medium (37°C) was added. The cells were incubated 24 hours at 37°C. At indicated time points, MFI of internalized CypHer5E was measured per well using homogeneous Fluorometric Microvolume Assay Technology (Applied Biosystems). As read out, fluorescence per cell was multiplied with the number of positive cells per well (counts x fluorescence).

Cytotoxicity assay

Mixed cell cultures were treated with ADC to simultaneously determine the amount of target cell kill and bystander kill. HER2, EGFR, and TF-expressing tumor cells were used as target cells and seeded (5,000 cells/well) in 96-well culture plates. Antigen-negative Jurkat cells were used as bystander cells and added to the plate (20,000 cells/well). To discriminate between both cell populations, Jurkat cells were labeled with CellTrace carboxy-fluorescein diacetate succinimidyl ester (CFSE) according to the manufacturer's instructions (Invitrogen). Next, serially diluted ADCs (10-0,000001 mg/mL) were added and the cells were incubated 4 days at 37°C. Cells were harvested and viability was assessed through live/dead staining on a flow cytometer. Target cell kill was plotted as the percentage of viable CFSE-negative cells. Bystander kill was plotted as the percentage of viable CFSE-positive cells.

Alternatively, 500,000 CFSE-labeled cells were cultured in T25 flasks (Greiner) in presence of 2 mg/mL ADC. After 3 days, the viable cells were harvested and analyzed for antigen expression using mouse TF (CLB), HER2 (R&D), and EGFR antibodies (BD) and goat anti-mouse IgG1-APC (Jackson). Each sample was spiked with 10,000 CFSE-negative Jurkat cells. During flow-cytometric analysis, the CFSE-negative Jurkat cells were gated and 3,000 events were measured in this gate, while all events were stored and analyzed.

Tumor xenograft models

Six- to 11-week-old female SCID mice (C.B-17/IcrPrkdc-scid/CRL) were purchased from Charles River. Subcutaneous tumors were induced by inoculation of 5×10^6 cells in the right flank of the mice. Tumor volumes were calculated from digital caliper measurements as $0.52 \times \text{length} \times \text{width}^2$ (mm³). When tumors reached 200 to 400 mm³, mice were grouped into groups of 7 mice with equal tumor size distribution and mAbs were injected intraperitoneally at indicated time points (1 or 4 mg/kg). During the study, blood samples were collected into heparin-containing tubes to confirm the presence of human IgG in plasma. IgG levels were quantified using a Nephelometer (Siemens Healthcare). Mice that did not show human IgG in plasma were excluded from the analysis. Some mice developing ulcerations not related to tumor size were euthanized for ethical reasons before the end of the study, which is indicated by the censored data points.

Statistical analysis

Data analysis was done using GraphPad Prism 5 software. Group data were reported as mean \pm SD. One-way ANOVA was applied for statistical analysis. Statistical analysis of xenograft studies was done with one-way ANOVA at the last day that all groups were complete. Mantel-Cox analysis of Kaplan-Meier curves was performed to analyze statistical differences in progression-free survival time.

Results

Tissue factor distribution in unstimulated tumor cells

In healthy tissue, TF is primarily expressed in intracellular pools and remains sequestered from circulating FVII (17, 18, 28). To determine TF distribution in cancer cells, we applied confocal microscopy. For this, we selected two cell lines based on aberrant expression of HER2 and TF (SK-OV-3, ovarian cancer) or EGFR

Table 1. Average number of molecules on plasma membrane

Cell line	Origin	TF (molecules/cell)	EGFR (molecules/cell)	HER2 (molecules/cell)
HCC1954	Breast cancer	400,000	100,000	600,000
A431	Epithelial cancer	200,000	500,000	30,000
SK-OV-3	Ovarian cancer	100,000	50,000	200,000
AU565	Breast cancer	20,000	100,000	500,000

NOTE: Average number of EGFR, HER2, and TF molecules expressed on the cell surface, calculated with quantitative flow cytometry as described in Supplementary Method S1.

and TF (A431, epithelial carcinoma), as depicted in Table 1. The cells were grown on glass coverslips, left unstimulated, and stained for TF, EGFR, and HER2. Markers of recycling endosomes (i.e., transferrin) and lysosomes (i.e., LAMP1) were included to determine compartmentalization of the different proteins. Figure 1A–C demonstrates that, in resting SK-OV-3 cells, TF is primarily localized intracellularly and partially colocalizes with the lysosomal marker LAMP1. EGFR and HER2 staining on the other hand was mainly localized to the plasma membrane.

Also in A431 cells (Fig. 1D) and HCC1954 cells (Supplementary Fig. S1), TF was more abundantly present in lysosomes as compared with EGFR and HER2, suggesting that TF has a high turnover in these tumor cells. This was confirmed by ELISA where total protein levels of TF, EGFR, and HER2 were measured in absence and presence of inhibitors of lysosomal degradation (Fig. 1E). Total protein levels of EGFR and HER2 were unaffected by addition of chloroquine, an inhibitor of endosomal acidification (29) or leupeptin, an inhibitor of lysosomal proteases. However, TF protein levels were increased

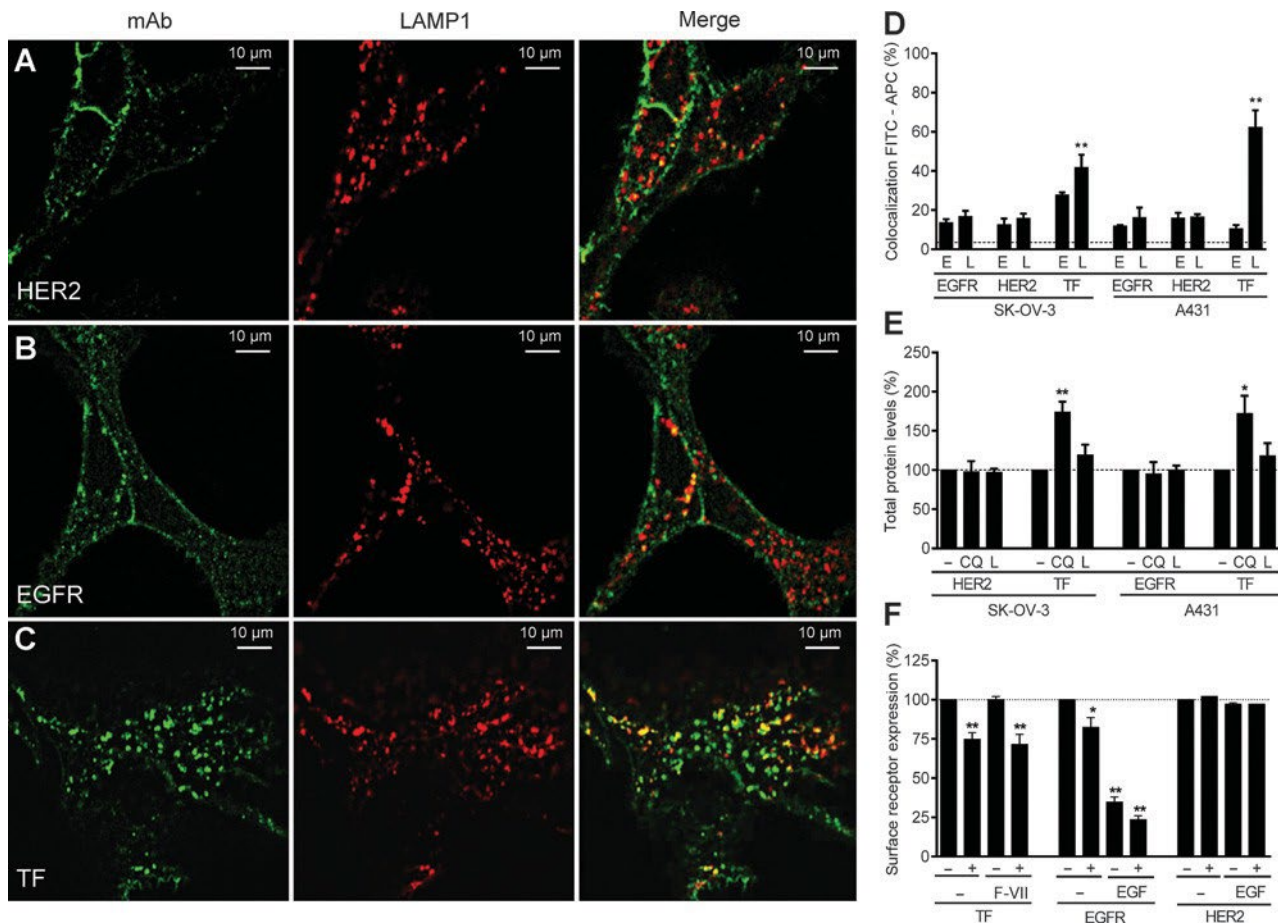


Figure 1. Distribution of HER2, EGFR, and TF in unstimulated tumor cells. A–C, confocal microscopy images (8-bit) of unstimulated SK-OV-3 cells. The left panel shows staining of HER2 (A), EGFR (B), and TF (C) with murine antibodies and goat anti-mouse IgG-FITC (green). In the middle panel, lysosomes were stained with mouse anti-human LAMP1-APC (red). The right panel shows the overlay (yellow). D, quantification of endosomal and lysosomal receptor colocalization. Each bar represents four different 12-bit images \pm SD. E, endosomes; L, lysosomes. E, downmodulation of total protein expression. Cells were incubated for 2 days with 100 mmol/L chloroquine or 100 mg/mL leupeptin, after which protein levels were measured with ELISA and expressed as percentage compared with untreated cells. Data, mean \pm SD. F, surface protein downmodulation on SK-OV-3 cells measured with quantitative flow cytometry. Cells were preincubated 30 minutes with (+) or without (-) monensin and incubated an additional 3 hours with 50 ng/mL EGF or 100 ng/mL FVIIa. Surface expression of remaining TF, EGFR, and HER2 was quantified and plotted as percentage relative to untreated cells. Data, mean \pm SD. *, $P < 0.05$; **, $P < 0.001$.

over 2-fold when lysosomal degradation was blocked with chloroquine, indicating that TF is continuously transported from endosomal to lysosomal compartments to undergo degradation. The enhanced colocalization of TF with transferrin (Fig. 1D) suggests that at least a part of the intracellular TF pool originated from the plasma membrane (30). Therefore we next investigated downmodulation of surface expressed receptors using quantitative flow cytometry. SK-OV-3 cells were incubated with the TF ligand FVIIa or the EGFR ligand EGF, after which residual receptor expression was quantified. Monensin was added to block transport of intracellular receptors to the cell surface and thereby trap internalized proteins in the cell. Figure 1F shows that FVIIa alone had no effect on surface expression of TF, whereas monensin significantly reduced TF expression, indicating that TF is constitutively recruited from intracellular pools to the plasma membrane. Previous reports have described the internalization of TF in presence of FVIIa (16, 31), our data demonstrate that TF is also internalized in absence of FVIIa. EGF on the other hand induced

significant downmodulation of surface expressed EGFR which was in line with previous reports (32), whereas HER2 expression was unaffected by EGF and monensin.

In summary, unlike EGFR and HER2, TF was continuously internalized and degraded, even in resting tumor cells. This suggests that the efficacy of TF-specific ADCs may be at least partly related to the endogenous internalization characteristics of TF.

Antibody binding to TF triggers internalization of mAb/TF-complexes

For certain receptors, antibody binding results in internalization of the Ab/receptor-complex (32). To investigate whether Ab/TF-complexes were internalized, we incubated SK-OV-3 and A431 cells for 3 hours at 37°C with antibodies directed against TF, EGFR, and HER2. The cells were cooled to 4°C and remaining extracellular proteins were quantified using noncompeting murine TF, EGFR, and HER2 antibodies. Fig. 2A demonstrates that TF-011 and TF-111 induced significant downmodulation of

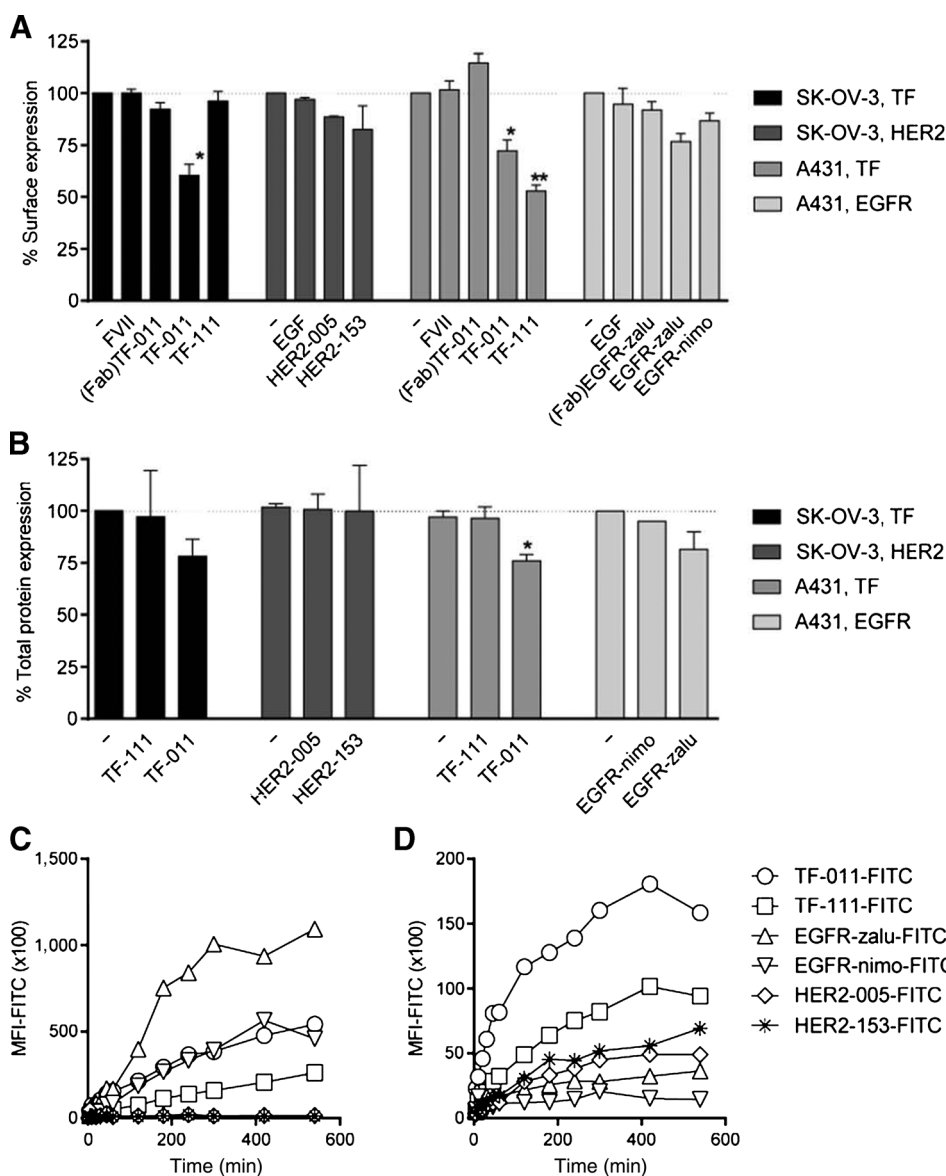


Figure 2. Antibody-mediated internalization and downmodulation of TF, EGFR, and HER2. A, downmodulation of surface-expressed proteins measured with flow cytometry. SK-OV-3 and A431 cells were incubated with 10 mg/mL antibody. After 3 hours, remaining surface expression of the different receptors was analyzed with quantitative flow cytometry and expressed as percentage relative to untreated cells. B, downmodulation of total protein levels. SK-OV-3 and A431 cells were incubated with 10 mg/mL antibody. After 2 days, protein levels were measured with ELISA and expressed as percentage compared with untreated cells. Data, mean \pm SD. C and D, intracellular accumulation of FITC-conjugated antibodies measured with flow cytometry. A431 (C) and SK-OV-3 (D) cells were incubated with 10 mg/mL Ab-FITC at 4°C and 37°C. At the indicated timepoints, extracellular bound Ab-FITC was removed through acid wash and MFI of intracellular FITC was analyzed with flow cytometry. One representative experiment out of three is shown. *, $P < 0.05$; **, $P < 0.001$.

extracellular TF, which was not observed with Fab fragments of mAb TF-011 or the TF physiologic ligand FVIIa. The tested EGFR and HER2 antibodies had no effect on extracellular expression of EGFR and HER2, respectively. The experiment was also performed in presence of the recycling inhibitor monensin. For EGFR and TF, this further decreased extracellular expression (data not shown). Next, it was investigated whether antibody-mediated downmodulation of extracellular proteins also results in downmodulation of total protein levels. SK-OV-3 and A431 cells were incubated for 2 days with EGFR, HER2, and TF antibodies, lysed and subjected to ELISA to measure the degree of protein. Figure 2B shows that TF-011 induced downmodulation of total TF protein in both cell lines. Also, a slight reduction of EGFR protein levels was observed upon incubation with EGFR antibody zalutumumab, but no effect on HER2 protein levels was observed with any of the HER2 antibodies.

To exclude that the reduced protein levels depicted in Fig. 2A result from antibody-induced shedding of TF, intracellular accumulation of FITC-conjugated antibodies was assessed to confirm that Ab/TF-complexes were indeed internalized. Cells were incubated with FITC-conjugated antibodies at 37°C for 0 to 9 hours. Before flow-cytometric analysis, extracellular FITC-conjugated antibodies were removed through acid wash and residual FITC fluorescence, originating from internalized FITC-conjugated antibodies, was measured on a flow cytometer. As depicted in Fig. 2C and D, both TF antibodies showed accumulation of FITC fluorescence over time, demonstrating that these antibodies were efficiently internalized.

TF/TF-011 complexes are rapidly targeted to the lysosomes

For an ADC-approach, it is typically required that internalized antibodies traffic to lysosomes where cellular proteases can initiate drug release (33). Using confocal microscopy, lysosomal transport of TF, EGFR, and HER2 antibodies was analyzed. SK-OV-3 and A431 cells were incubated with the indicated antibodies, and after 1 or 16 hours, cells were fixed, permeabilized, and stained with FITC-conjugated goat- α -human IgG1. After one hour, TF-011 already demonstrated clear internalization and lysosomal colocalization (Fig. 3A). EGFR antibody zalutumumab was also internalized after one hour, but the internalized antibody had not yet reached the lysosomes (Fig. 3C), whereas HER2 antibody 005 only stained at the plasma membrane (Fig. 3E). After 16 hours, all antibodies demonstrated substantial internalization and lysosomal colocalization, but TF mAbs were most abundantly present in lysosomes (Fig. 3B, D, F, and G). In addition, receptor distribution was tested after antibody treatment (Supplementary Fig. S2). Both TF antibodies significantly increased the amount of TF in endosomes and lysosomes of SK-OV-3 and A431 cells. EGFR mAbs zalutumumab and nimotuzumab also enhanced endosomal and lysosomal colocalization of EGFR in A431 cells. In contrast, cellular distribution of HER2 was hardly affected by HER2 antibodies 005 and 153.

The more rapid lysosomal colocalization of TF-mAbs led us to investigate TF-mediated internalization and lysosomal targeting in more detail. By conjugating TF, HER2, and EGFR mAbs with CypHer5E, a dye that becomes fluorescent at acidic pH, we were able to follow internalization and lysosomal colocalization over time. Both endosomes and lysosomes are acidic environments that induce fluorescence of CypHer5E. To distinguish between fluorescence resulting from endosomal and lysosomal transport, SK-OV-3 cells were preincubated with chloroquine, which inhi-

bits the acidification and fusion of endosomes with lysosomes (34). Thus, inhibition of CypHer5E fluorescence by chloroquine is indicative of lysosomal transport. This was most evident for TF-011 (Fig. 3H). Although fluorescence of CypHer5E-conjugated mAbs 005, 153, and zalutumumab was only inhibited after 24-hour incubation (Fig. 3I–K), fluorescence of TF-011-CypHer5E was already inhibited within one hour. This shows that TF-bound antibodies were rapidly transported to lysosomes, whereas lysosomal transport of EGFR and HER2 mAbs was relatively slow.

In vitro cytotoxicity induced by duostatin-3-conjugated TF, EGFR, and HER2 antibodies

To investigate whether the more rapid lysosomal targeting observed with TF mAbs, results in increased cytotoxicity of TF-directed ADCs, we conjugated antibodies TF-011, 005, and zalutumumab with duostatin-3 using a valine-citrulline linker that is cleaved by intracellular proteases such as cathepsin B. Duostatin-3 is an antimetabolic agent that inhibits cell division by blocking of tubulin polymerization. Unlike vcMMAE, duostatin-3 cannot kill neighboring tumor cells when the drug is released from the antibody. This was also demonstrated in Fig. 4B, D, and F, where duostatin-3-conjugated antibodies did not induce bystander kill. Whereas TF-011-MMAE induced potent bystander kill which was in line with results published previously (4, 33). To study the target requirements needed for efficient intracellular drug delivery, a drug-linker that only affects antigen-expressing cells was preferred. Figure 4A, C, and E shows that duostatin-3-conjugated HER2 and EGFR antibodies only induced cytotoxicity when tumor cells highly overexpress their targets HER2 (AU565 and SK-OV-3) and EGFR (A431 and AU565), respectively. Viability of tumor cells that display moderate overexpression of HER2 (A431) or EGFR (SK-OV-3) was hardly affected. In contrast, TF-mAbs conjugated with duostatin-3 induced cytotoxicity in all tested cell lines, including cells that express less than 20,000 TF molecules/cell. Analysis of TF expression in SK-OV-3 cells that survived TF-ADC treatment demonstrated that TF expression was similar before and after treatment (Table 2 and Supplementary Fig. S3). However, the proliferation rate of the surviving cells was reduced, as indicated by the high CFSE fluorescence of the surviving cells. This indicates that lack of efficacy against these cells was caused by their low proliferation rate, rather than lack of target expression.

Antitumor activity of duostatin-3-conjugated TF, EGFR, and HER2 antibodies *in vivo*

Finally, the effect of ADC treatment on tumor growth was assessed *in vivo*. The ADCs were compared in two different tumor xenograft models, starting with the breast cancer model HCC1954 (Fig. 5A and B) which highly overexpressed HER2 and TF (Table 1). Figure 5B demonstrates that treatment with a single dose of 1 mg/kg TF-ADC resulted in significant inhibition of HCC1954 tumor growth as compared with animals treated with isotype control ADC. At the same dose, HER2-ADC had no effect on tumor growth. At 4 mg/kg, both ADCs induced tumor regression, which was sustained until at least 67 days after treatment.

Using the epidermal carcinoma model A431, ADCs targeting TF and EGFR were compared (Fig. 5C and D). A single dose of 1 mg/kg TF-ADC induced significant inhibition of tumor growth, which was increased at 4 mg/kg. EGFR-ADC only reduced tumor

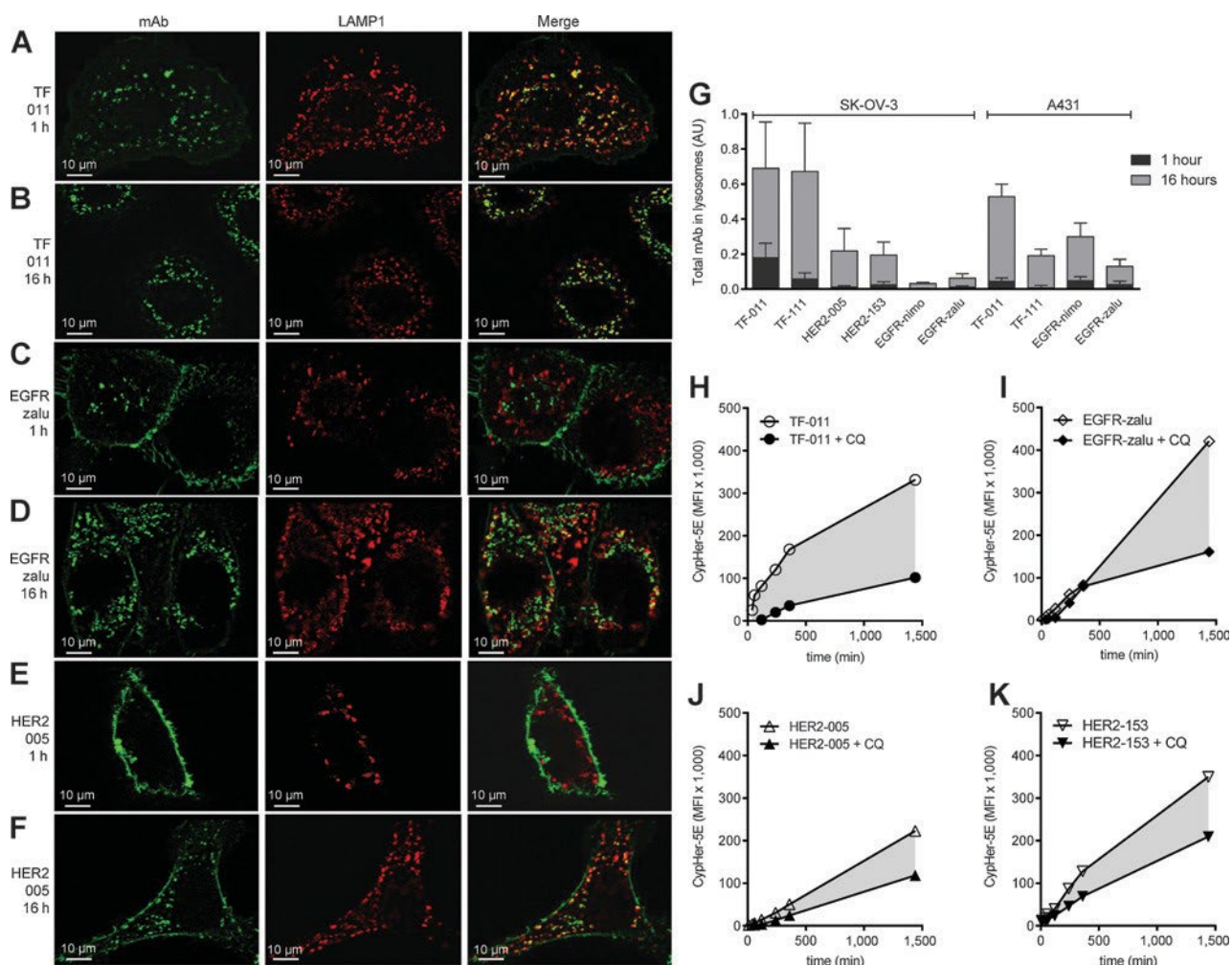


Figure 3.

Lysosomal colocalization of TF, EGFR, and HER2 antibodies. A–F, confocal microscopy analysis of SK-OV-3 (A and B, E and F) and A431 (C and D) cells demonstrating fast and increased lysosomal transport of TF-011. Lysosomes were stained with mouse anti-human LAMP1-APC (red). Zalutumumab (anti-EGFR), 005 (anti-HER2), and TF-011 (anti-TF) were detected with goat anti-human IgG1-FITC (green). G, arbitrary units (AU) represent the total pixel intensity of antibody overlapping with the lysosomal marker LAMP1, divided by the total pixel intensity of LAMP1. Data, mean \pm SD of four images. H and K, lysosomal targeting of CypHer5E-conjugated mAbs. SK-OV-3 cells, preincubated with or without 100 mmol/L chloroquine, were incubated with CypHer5E-conjugated antibodies: TF-011 (H), zalutumumab (I), 005 (J), and 153 (K). At the indicated time points, CypHer5E fluorescence was measured using homogeneous Fluorometric Microvolume Assay Technology. The gray area indicates antibody present in lysosomal compartments.

growth at 4 mg/kg, a dose at which TF-ADC treatment was significantly more effective. Overall, TF-ADC treatment induced significant inhibition of tumor growth. Despite the reduced expression of TF as compared with HER2 and EGFR, TF-ADC outperformed HER2- and EGFR-ADCs. Hence, these data demonstrate the potential of TF as tumor target for an ADC approach.

Discussion

Antibodies conjugated with tubulin inhibitors have demonstrated impressive preclinical and clinical antitumor activity (1, 20, 35, 36). However, the optimal target characteristics for ADC development are not entirely clear. Most ADCs are dependent on internalization and lysosomal targeting to release their cytotoxic compound. Thus, the internalization characteristics of a tumor target may greatly contribute to the efficacy of ADCs directed against that target. In addition, binding of antibodies

or ADCs to specific tumor targets may change the internalization characteristics of the tumor target. In this study, the internalization characteristics of three different tumor targets, TF, EGFR, and HER2, as well as antibodies and ADCs specific for those targets, were compared. Internalization, lysosomal sorting and intracellular degradation of the three proteins were analyzed in absence and presence of monoclonal antibodies. The combination of TF and antibody TF-011 was the only combination demonstrating efficacy in all assays. TF demonstrated significant and constitutive internalization, lysosomal colocalization and degradation in tumor cells, all of which were increased upon incubation with TF-011. Given the potential of TF as target for an ADC approach, TF-, EGFR-, and HER2-mAbs were conjugated with the cleavable linker-drug vcDuostatin-3, generating ADCs that provide specific tumor targeting with a payload only affecting proliferating cells. We found that TF-ADC outperformed HER2-ADC and EGFR-ADC in two different tumor xenograft models.

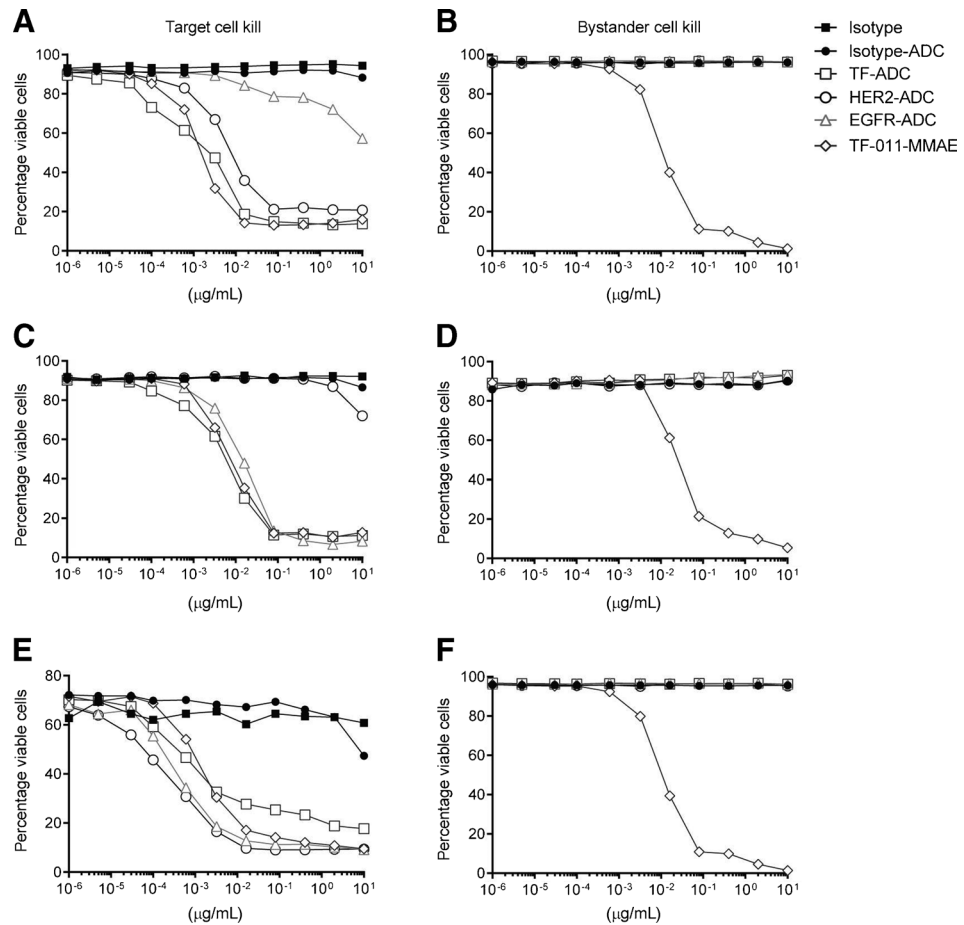


Figure 4. Cytotoxicity of TF-ADC, EGFR-ADC, HER2-ADC, and TF-011-MMAE *in vitro*. SK-OV-3 (A and B), A431 (C and D), and AU565 (E and F) cells were seeded in 96-well tissue culture plates together with CFSE-labeled Jurkat cells. Serially diluted ADCs and isotype control antibody were added to the cells. After 4 days incubation at 37°C viability was assessed on a flow cytometer. Target cell kill was plotted as the percentage of viable CFSE⁺ SK-OV-3, A431, and AU565 cells (left). Bystander kill was plotted as the percentage of viable CFSE⁺ cells (right).

Quantitative flow-cytometric analysis of tumor cell lines revealed that, like EGFR and HER2, TF can be aberrantly expressed on tumor cells. Compared with normal melanocytes, more than 1,000-fold increased TF expression has been reported on metastatic human melanoma cells (37). In the tumor models selected here, extracellular expression of TF was lower compared with EGFR and HER2. However, despite the lower antigen expression, the antitumor activity of TF-ADC was

more potent compared with HER2- and EGFR-ADCs. This can be explained by the efficient transport of TF-011 from the plasma membrane into lysosomes of tumor cells as demonstrated with confocal microscopy. Previous publications also indicate that TF has a higher turnover rate compared with EGFR and HER2. Hamik and colleagues demonstrated that the half-life of TF on monocytes was 3.7 hours, which could be reduced to 1.3 hours when TF was bound by TF protein inhibitor and FVII (38). Unstimulated EGFR and HER2 on the other hand have a half-life of 6 to 24 hours depending on the cell line used (39). Because TF is the main physiologic initiator of the coagulation cascade, which represents a system that needs to be tightly regulated, it makes sense that TF is more efficiently internalized and degraded compared with EGFR and HER2.

Internalization of TF has been studied previously (16, 40) and is believed to be an active process which can be enhanced through binding of FVIIa. We did not observe FVIIa-mediated internalization of TF. Instead, we found that TF was constitutively being turned over on tumor cells, a process that was not influenced by presence of FVIIa. Most studies focussing on internalization of TF: FVIIa complexes made use of radiolabeled FVIIa (16, 31, 41). Our studies, using TF expression as read out, demonstrate that FVIIa most likely piggybacks with internalizing TF. Various cancer cells, including ovarian cancer cells, have been reported to produce FVII themselves (42); however, we did not detect FVII production in culture supernatant (data not shown).

Table 2. Flow-cytometric analysis of SK-OV-3 cells after ADC treatment

	Cytotoxicity (number of events)	Antigen expression (MFI APC)	Proliferation rate (MFI CFSE)
EGFR	40,100	26,613	65,493
EGFR β EGFR-ADC	17,858	21,380	93,951
HER2	39,836	90,735	65,493
HER2 β HER2-ADC	7,034	76,490	122,213
TF	42,522	51,237	65,493
TF β TF-ADC	2,403	45,816	175,662

NOTE: SK-OV-3 cells were labeled with CFSE, a dye that is stably fluorescent and that is transferred to daughter cells upon cell division with its fluorescence being halved. Thus, reduced CFSE fluorescence indicates SK-OV-3 proliferation. CFSE-labeled cells were treated 3 days with 2 mg/mL ADC, after which cytotoxicity was analyzed as well as expression of the antigen targeted by the respective ADC. Cytotoxicity was expressed as number of events measured on a flow cytometer. Antigen expression was detected with mouse anti-HER2, anti-EGFR, and anti-TF antibodies in combination with APC-conjugated rabbit anti-mouse and depicted as MFI of APC.

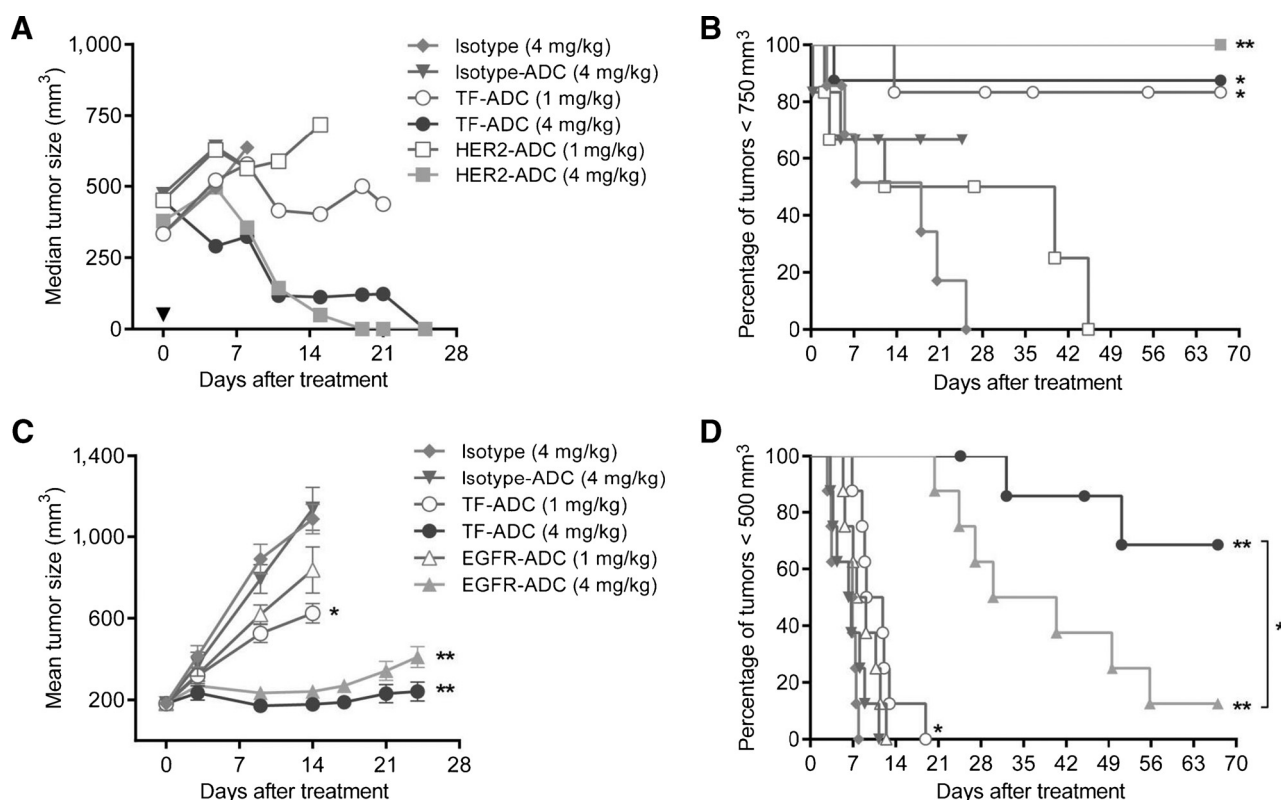


Figure 5.

Efficacy of TF-ADC, HER2-ADC, and EGFR-ADC in tumor xenograft models. Mice were inoculated subcutaneously with 5×10^6 HCC1954 (A and B) or A431 (C and D) cells. When average tumor volume reached $>200 \text{ mm}^3$, mice were divided in groups of 7 mice with equal tumor size distribution and injected intraperitoneally at indicated time points with 4 mg/kg or 1 mg/kg mAb or ADC. Tumors were measured twice a week by using calipers, and the median (A) or mean \pm SE (C) tumor volume (mm^3) was plotted against time, as well as time to progression indicated by the percentage of tumors $<750 \text{ mm}^3$ (B) or $<500 \text{ mm}^3$ (D). In the HCC1954 model, some mice developed ulcerations unrelated to tumor size or Ab-treatment. These mice were withdrawn from the study as indicated by the censored data points (B). Median tumor volumes were not calculated when more than 3 mice had been withdrawn (A). *, $P < 0.05$; **, $P < 0.001$.

Although the more rapid internalization and lysosomal targeting of TF seem fundamental for effective ADC treatment, the potent antitumor effect of TF-ADC cannot be fully ascribed to the target characteristics of TF alone. Antibody selection plays an important role as well. This was illustrated by the increased internalization and lysosomal targeting observed with TF-011. Although TF-011 is expected to crosslink extracellular TF, Fab-011 and FVII lack the ability to crosslink TF, indicating that mAb-induced crosslinking may be critical to increase downmodulation of extracellular TF. TF-111, on the other hand, only seems to crosslink TF when highly overexpressed. Moreover, differential antibody binding at low pH may influence intracellular trafficking of ADCs and consequently increase their lysosomal transport. Flow-cytometric analysis of antibody binding at pH6 and pH7.4 revealed no differences in binding at reduced pH (Supplementary Table S1). Also, no substantial differences were observed between apparent affinities of antibodies targeting TF, EGFR, and HER2 (Supplementary Table S1). The low-affinity EGFR mAb nimotuzumab was an exception to this and showed low apparent affinity binding to EGFR-expressing cells (EC_{50} value 15.6 nmol/L). Furthermore, inhibition of receptor signaling and engagement of immune effector cells may contribute to the antitumor activity of ADCs as well. However, treatment of established A431 xenografts with comparable dosing of unconjugated mAbs induced significantly less (EGFR-mAb; ref. 43) or no (TF-mAbs; ref. 4),

inhibition of tumor growth. The unconjugated HER2 antibody 005 demonstrated modest inhibition of *in vivo* tumor growth, when tested at >10 -fold higher dose in a high HER2-expressing tumor model (data not shown).

Although EGFR and HER2 belong to a family of receptor tyrosine kinases, for which endocytic trafficking has been extensively investigated, TF is a member of the class II cytokine receptor superfamily. To date, little is known about intracellular trafficking of these proteins and their potential use in ADC-based therapy. Our data indicate that such targets can be very attractive for an ADC approach because of their rapid internalization, lysosomal targeting, and degradation, which may be inherent to their physiologic roles in regulating immune responses (44, 45). Taken together, these data support the use of TF-ADC in cancer therapy and a clinical study is underway to assess the safety and efficacy of TF-011-MMAE, an auristatin-conjugate of antibody TF-011, for the treatment of patients with solid cancers.

Disclosure of Potential Conflicts of Interest

B.E.C.G. de Goeij has ownership interest as coauthor of patent applications and owner of warrants with Genmab. D. Satijn has ownership interest as coauthor of patent applications and owner of warrants with Genmab. P.H.C. van Berkel has ownership interest (including patents) in Genmab. P.W.H.I. Parren has ownership interest (including patents) in Genmab. No potential conflicts of interest were disclosed by the other authors.

Authors' Contributions

Conception and design: B.E.C.G. de Goeij, D. Satijn, W.K. Bleeker, P.H.C. van Berkel, P.W.H.I. Parren
 Development of methodology: B.E.C.G. de Goeij, C.M. Freitag, A. Khasanov, T. Zhu, G. Chen, D. Miao
 Acquisition of data (provided animals, acquired and managed patients, provided facilities, etc.): C.M. Freitag, W.K. Bleeker
 Analysis and interpretation of data (e.g., statistical analysis, biostatistics, computational analysis): B.E.C.G. de Goeij, W.K. Bleeker, A. Khasanov, T. Zhu, P.W.H.I. Parren
 Writing, review, and/or revision of the manuscript: B.E.C.G. de Goeij, W.K. Bleeker, A. Khasanov, T. Zhu, P.H.C. van Berkel, P.W.H.I. Parren
 Administrative, technical, or material support (i.e., reporting or organizing data, constructing databases): B.E.C.G. de Goeij, R. Wubbolts, A. Khasanov, T. Zhu, G. Chen

Study supervision: D. Satijn, W.K. Bleeker, P.W.H.I. Parren
 Other (collaborator): D. Miao

Acknowledgments

The authors thank Maarten Dokter, Hendrik ten Napel, and Ester van't Veld for technical support and Esther Breij for reviewing the article.

The costs of publication of this article were defrayed in part by the payment of page charges. This article must therefore be hereby marked *advertisement* in accordance with 18 U.S.C. Section 1734 solely to indicate this fact.

Received September 17, 2014; revised January 29, 2015; accepted January 29, 2015; published OnlineFirst February 27, 2015.

References

- Senter PD, Sievers EL. The discovery and development of brentuximab vedotin for use in relapsed Hodgkin lymphoma and systemic anaplastic large cell lymphoma. *Nat Biotechnol* 2012;30:631–7.
- LoRusso PM, Weiss D, Guardino E, Girish S, Sliwkowski MX. Trastuzumab emtansine: a unique antibody–drug conjugate in development for human epidermal growth factor receptor 2-positive cancer. *Clin Cancer Res* 2011;17:6437–47.
- Burris HA. Trastuzumab emtansine: a novel antibody–drug conjugate for HER2-positive breast cancer. *Expert Opin Biol Ther* 2011;11:807–19.
- Breij EC, de Goeij BE, Verploegen S, Schuurhuis DH, Amirkhosravi A, Francis J, et al. An antibody–drug conjugate that targets tissue factor exhibits potent therapeutic activity against a broad range of solid tumors. *Cancer Res* 2014;74:1214–26.
- Goldin-Lang P, Tran QV, Fichtner I, Eisenreich A, Antoniuk S, Schulze K, et al. Tissue factor expression pattern in human non-small cell lung cancer tissues indicate increased blood thrombogenicity and tumor metastasis. *Oncol Rep* 2008;20:123–8.
- Shigemori C, Wada H, Matsumoto K, Shiku H, Nakamura S, Suzuki H. Tissue factor expression and metastatic potential of colorectal cancer. *Thromb Haemost* 1998;80:894–8.
- Gonzalez-Gronow M, Gawdi G, Pizzo SV. Tissue factor is the receptor for plasminogen type 1 on 1-LN human prostate cancer cells. *Blood* 2002;99:4562–7.
- Patry G, Hovington H, Larue H, Harel F, Fradet Y, Lacombe L. Tissue factor expression correlates with disease-specific survival in patients with node-negative muscle-invasive bladder cancer. *Int J Cancer* 2008;122:1592–7.
- Uno K, Homma S, Satoh T, Nakanishi K, Abe D, Matsumoto K, et al. Tissue factor expression as a possible determinant of thromboembolism in ovarian cancer. *Br J Cancer* 2007;96:290–5.
- Cocco E, Hu Z, Richter CE, Bellone S, Casagrande F, Bellone M, et al. h1-con1, a factor VII-IgGFc chimeric protein targeting tissue factor for immunotherapy of uterine serous papillary carcinoma. *Br J Cancer* 2010;103:812–9.
- Cocco E, Varughese J, Buza N, Bellone S, Glasgow M, Bellone M, et al. Expression of Tissue factor in Adenocarcinoma and Squamous Cell Carcinoma of the Uterine Cervix: Implications for immunotherapy with h1-con1, a factor VII-IgGFc chimeric protein targeting tissue factor. *BMC Cancer* 2011;11.
- Khorana AA, Ahrendt SA, Ryan CK, Francis CW, Hruban RH, Hu YC, et al. Tissue factor expression, angiogenesis, and thrombosis in pancreatic cancer. *Clin Cancer Res* 2007;13:2870–5.
- Wojtkiewicz MZ, Zacharski LR, Rucinska M, Zimnoch L, Jaromin J, Rozanska-Kudelska M, et al. Expression of tissue factor and tissue factor pathway inhibitor in situ in laryngeal carcinoma. *Thromb Haemost* 1999;82:1659–62.
- Hamada K, Kuratsu J, Saitoh Y, Takeshima H, Nishi T, Ushio Y. Expression of tissue factor in glioma. *Noshuyo Byori* 1996;13:115–8.
- Jiang X, Zhu S, Panetti TS, Bromberg ME. Formation of tissue factor-factor VIIa-factor Xa complex induces activation of the mTOR pathway which regulates migration of human breast cancer cells. *Thromb Haemost* 2008;100:127–33.
- Hansen CB, Pyke C, Petersen LC, Rao LV. Tissue factor-mediated endocytosis, recycling, and degradation of factor VIIa by a clathrin-independent mechanism not requiring the cytoplasmic domain of tissue factor. *Blood* 2001;97:1712–20.
- Mandal SK, Pendurthi UR, Rao LV. Cellular localization and trafficking of tissue factor. *Blood* 2006;107:4746–53.
- Schecter AD, Giesen PL, Taby O, Rosenfeld CL, Rossikhina M, Fyfe BS, et al. Tissue factor expression in human arterial smooth muscle cells. TF is present in three cellular pools after growth factor stimulation. *J Clin Invest* 1997;100:2276–85.
- Kasthuri RS, Taubman MB, Mackman N. Role of tissue factor in cancer. *J Clin Oncol* 2009;27:4834–8.
- Verma S, Miles D, Gianni L, Krop IE, Welslau M, Baselga J, et al. Trastuzumab Emtansine for HER2-Positive Advanced Breast Cancer. *N Eng J Med* 2012;367:1783–91.
- Fishwild DM, O'Donnell SL, Bengoechea T, Hudson DV, Harding F, Bernhard SL, et al. High-avidity human IgG kappa monoclonal antibodies from a novel strain of minilocus transgenic mice. *Nat Biotechnol* 1996;14:845–51.
- de Goeij BE, Peipp M, De Haij S, van den Brink EN, Kellner C, Riedl T, et al. HER2 monoclonal antibodies that do not interfere with receptor heterodimerization-mediated signaling induce effective internalization and represent valuable components for rational antibody–drug conjugate design. *MABs in press* [published online January 3, 2014; doi:10.1617/mabs27705].
- Bleeker WK, Lammerts van Bueren JJ, van Ojik HH, Gerritsen AF, Ployter M, Houtkamp M, et al. Dual mode of action of a human anti-epidermal growth factor receptor monoclonal antibody for cancer therapy. *J Immunol* 2004;173:4699–707.
- Ramakrishnan MS, Eswaraiah A, Crombet T, Piedra P, Saurez G, Iyer H, et al. Nimotuzumab, a promising therapeutic monoclonal for treatment of tumors of epithelial origin. *MABs* 2009;1:41–8.
- Levkowitz G, Waterman H, Zamir E, Kam Z, Oved S, Langdon WY, et al. c-Cbl/Sli-1 regulates endocytic sorting and ubiquitination of the epidermal growth factor receptor. *Genes Dev* 1998;12:3663–74.
- Poncelet P, Carayon P. Cytofluorometric quantification of cell-surface antigens by indirect immunofluorescence using monoclonal antibodies. *J Immunol Methods* 1985;85:65–74.
- Labrijn AF, Meesters JI, de Goeij BE, van den Bremer ET, Neijssen J, van Kampen MD, et al. Efficient generation of stable bispecific IgG1 by controlled Fab-arm exchange. *Proc Natl Acad Sci U S A* 2013;110:5145–50.
- Mandal SK, Pendurthi UR, Rao LV. Tissue factor trafficking in fibroblasts: involvement of protease-activated receptor-mediated cell signaling. *Blood* 2007;110:161–70.
- Vincent MJ, Bergeron E, Benjannet S, Erickson BR, Rollin PE, Ksiazek TG, et al. Chloroquine is a potent inhibitor of SARS coronavirus infection and spread. *Virology* 2005;2:69.
- Mellman I. Endocytosis and molecular sorting. *Annu Rev Cell Dev Biol* 1996;12:575–625.
- Iakhiaev A, Pendurthi UR, Voigt J, Ezban M, Vijaya Mohan Rao L. Catabolism of factor VIIa bound to tissue factor in fibroblasts in the presence

- and absence of tissue factor pathway inhibitor. *J Biol Chem* 1999; 274:36995–7003.
32. Lammerts van Bueren JJ, Bleeker WK, Bogh HO, Houtkamp M, Schuurman J, van de Winkel JG, et al. Effect of target dynamics on pharmacokinetics of a novel therapeutic antibody against the epidermal growth factor receptor: implications for the mechanisms of action. *Cancer Res* 2006;66:7630–8.
 33. Smith LM, Nesterova A, Alley SC, Torgov MY, Carter PJ. Potent cytotoxicity of an auristatin-containing antibody–drug conjugate targeting melanoma cells expressing melanotransferrin/p97. *Mol Cancer Ther* 2006;5:1474–82.
 34. Koh YH, von Arnim CA, Hyman BT, Tanzi RE, Tesco G. BACE is degraded via the lysosomal pathway. *J Biol Chem* 2005;280:32499–504.
 35. Flygare JA, Pillow TH, Aristoff P. Antibody–drug conjugates for the treatment of cancer. *Chem Biol Drug Des* 2013;81:113–21.
 36. Alley SC, Okeley NM, Senter PD. Antibody–drug conjugates: targeted drug delivery for cancer. *Curr Opin Chem Biol* 2010;14:529–37.
 37. Mueller BM, Reisfeld RA, Edgington TS, Ruf W. Expression of tissue factor by melanoma cells promotes efficient hematogenous metastasis. *Proc Natl Acad Sci U S A* 1992;89:11832–6.
 38. Hamik A, Setiadi H, Bu G, McEver RP, Morrissey JH. Down-regulation of monocyte tissue factor mediated by tissue factor pathway inhibitor and the low density lipoprotein receptor-related protein. *J Biol Chem* 1999;274:4962–9.
 39. Sorkin A, Goh LK. Endocytosis and intracellular trafficking of ErbBs. *Exp Cell Res* 2008;314:3093–106.
 40. Rao LVM, Pendurthi UR. Regulation of tissue factor-factor VIIa expression on cell surfaces: A role for tissue factor-factor VIIa endocytosis. *Mol Cell Biochem* 2003;253:131–40.
 41. Chang GT, Kisiel W. Internalization and degradation of recombinant human coagulation factor VIIa by the human hepatoma cell line HuH7. *Thromb Haemost* 1995;73:231–8.
 42. Yokota N, Koizume S, Miyagi E, Hirahara F, Nakamura Y, Kikuchi K, et al. Self-production of tissue factor-coagulation factor VII complex by ovarian cancer cells. *Br J Cancer* 2009;101:2023–9.
 43. Overdijk MB, Verploegen S, van den Brakel JH, Lammerts van Bueren JJ, Vink T, van de Winkel JG, et al. Epidermal growth factor receptor (EGFR) antibody-induced antibody-dependent cellular cytotoxicity plays a prominent role in inhibiting tumorigenesis, even of tumor cells insensitive to EGFR signaling inhibition. *J Immunol* 2011;187:3383–90.
 44. Ragimbeau J, Dondi E, Alcover A, Eid P, Uze G, Pellegrini S. The tyrosine kinase Tyk2 controls IFNAR1 cell surface expression. *EMBO J* 2003;22:537–47.
 45. Wei SH, Ming-Lum A, Liu Y, Wallach D, Ong CJ, Chung SW, et al. Proteasome-mediated proteolysis of the interleukin-10 receptor is important for signal downregulation. *J Interferon Cytokine Res* 2006; 26:281–90.